Journal of the European Ceramic Society **11** (1993) 51–62

Creep Properties of an Alumina–Zirconia Composite Reinforced with Silicon Carbide Whiskers

M. Backhaus-Ricoult & P. Eveno

Laboratoire de Physique des Matériaux, CNRS-Bellevue, 92195 Meudon, France

(Received 22 April 1992; accepted 8 May 1992)

Abstract

The compressive creep behaviour of a ceramic composite consisting of a zirconia-toughened alumina matrix reinforced with silicon carbide whiskers is studied between 1550 and 1673 K in different atmospheres and at stresses ranging from 10 to 250 MPa. Macroscopic parameters, like the deformation rate, the stress exponent and the activation energy, are determined. At 1573 K, steady-state creep rates between $10^{-8}\,s^{-1}$ (30 MPa) and $10^{-6}\,s^{-1}$ (200 MPa) are measured with only minor differences for reducing neutral and oxidizing atmospheres. At 1573 K and above a given stress threshold, a stress exponent of 2 and an activation energy of 800 kJ mol^{-1} are measured. At higher temperatures and above this stress threshold, the stress exponent is 2·5. Electron microscopy observations of the deformed material reveal cavities at triple junctions and stress whirls at grain boundaries. The dislocation density is not found to be increased during creep. Therefore, grain boundary sliding, compensated by diffusion along the interfaces and grain boundaries, and cavitation are considered to be the main mechanisms contributing to the deformation of the composite. At high temperature, microcracking also contributes to the deformation.

Das Kriechverhalten eines Siliziumkarbid–Zirkoniumdioxid–Aluminiumoxid-Verbundwerkstoffes wird für verschiedene Atmosphären im Temperaturbereich von 1550 bis 1673 K für verschiedene Spannungen zwischen 10 und 250 MPa untersucht. Für 1573 K treten Kriechgeschwindigkeiten zwischen $10^{-8}\,s^{-1}$ (30 MPa) und $10^{-6}\,s^{-1}$ (200 MPa) auf, oberhalb einer Mindestspannung werden ein Spannungsexponent von 2 und eine Aktivierungsenergie von 800 kJ mol^{-1} gemessen. Bei höherer Temperatur steigt der Spannungsexponent im Bereich höherer Spannungen auf 2·5. Das Kriechverhalten wird nur wenig von der Atmosphäre beeinflußt. Elektronenmikroskopische Untersuchungen an verformten Proben zeigen, daß die Versetzungsdichte beim Kriechen nicht ansteigt und daß sich Spannungszentren an Korngrenzen und Poren in Tripelpunkten bilden. Daher können Korngrenzgleiten, kompensiert durch Diffusion entlang von Korn- und Phasengrenzen, sowie Porenbildung als die zum Kriechen beitragenden Kriechmechanismen angesehen werden.

Le fluage d'un composite a base d'alumine, zircone et carbure de silicium est étudié entre 1550 et 1673 K pour des contraintes de 10 à 250 MPa dans différentes atmosphères. L'influence de l'atmosphère sur le fluage est faible. A 1573 K, la vitesse de fluage varie entre $10^{-8}\,s^{-1}$ (30 MPa) et $10^{-6}\,s^{-1}$ (200 MPa). Au-dessus d'un seuil de contrainte, l'exposant de contrainte est 2 (2·5 pour des températures plus élevées) et l'énergie d'activation est 800 kJ mol^{-1}. L'observation des échantillons déformés par microscopie électronique à transmission a montré que la densité de dislocations n'augmente pas pendant le fluage. Des concentrations de contrainte sont observées au niveau des joints de grains et des cavités situées aux points triples. Nous proposons donc que le mécanisme de fluage est essentiellement un glissement aux joints de grains, compensé par la diffusion le long de ces joints et des interfaces, ainsi que par de la cavitation. A température élevée, la microfissuration devient importante.

1 Introduction

Whisker-reinforced ceramics find applications in high-temperature structural engineering. For these technical applications, ceramic composites display a much higher corrosion resistance (especially in air) than metals do. At the same time, they are also far more mechanically reliable than monolithic ceramics. Silicon carbide whiskers can improve both the fracture strength and the fracture toughness of

Journal of the European Ceramic Society 0955-2219/93/$6.00

the composite, because of their high Young's modulus and of the resulting strengthening mechanisms which prevent catastrophic brittle failure of the material, occurring by crack propagation. Depending on the chemistry and the grain size of the matrix, as well as on the geometry, surface chemistry and surface roughness of the whiskers, the strengthening may be more or less efficient. Crack deflection, whisker pull-out and whisker bridging, related to unbonding of the whisker–matrix interface, are among the mechanisms held responsible for the toughening effect.[1]

Silicon carbide whiskers are used to reinforce various matrix materials, such as alumina,[2-5] silicon nitride[6-8] or mullite,[9,10] for instance. Among those composites, reinforced alumina is used for the fabrication of cutting tools[11] and could be used in the fabrication of specific ceramic engine parts, such as pump seals or shielding plates. This material is already fabricated by several academic and industrial research groups and is always reported to display a remarkably higher room-temperature toughness than monolithic alumina.[2,12,13] Low-temperature toughness and strength are particularly studied as functions of whisker content,[14,15] whisker size[14] and total density of the composite.[3] Investigations of the microstructure of these composites are reported in the literature.[4,14,16,17] Whether or not an amorphous layer is observed at the interface between silicon carbide whiskers and alumina matrix depends on the way the composite has been processed by the various authors.[4,14,18-20] Similarly, the presence of glassy pockets within the matrix seems to be strongly related to the use of additives during fabrication.

For technical applications at high temperature, not only the toughness of the material but also its corrosion and creep behaviour become critical for its reliability. A number of studies have focused on these topics and are now summarized.

The oxidation behaviour of silicon carbide reinforced alumina is investigated in Refs 4, 17 and 21. Kinetics, microstructural evolution and oxidation mechanism for the alumina–zirconia composite reinforced with silicon carbide whiskers, the material investigated in the present work, are discussed in Ref. 22.

The creep behaviour of silicon carbide reinforced alumina composites is mainly studied by bending tests at high temperature.[4,18,19,23,24] All authors report a strengthening of the composite compared to pure alumina, associated with a two order of magnitude decrease of the flexural creep rate. The creep rate appears to depend strongly on the fabrication of the composite[4,18-20] and only slightly on the whisker content (decreasing strain rate with increasing whisker content[14]).

The absolute values given in the literature for the strain rate of the composite at a given temperature and stress vary widely from one author to another.[14,19,25] Lin & Becher report reliable values for the creep rate of an alumina–20% silicon carbide composite:[24] $10^{-8}\,s^{-1}$ at 1573 K and 100 MPa, and $3 \times 10^{-8}\,s^{-1}$ at 1673 K and 100 MPa. Depending on the authors, stress exponents between 1 and 8 are reported.[4,14,19,25] An increase of the stress exponent with creep temperature and applied stress is observed in most cases. Large discrepancies exist as well among reports about microstructural changes during creep. Whereas some authors report high dislocation densities in deformed samples, which have developed during creep,[4] others mention the absence of any dislocation activity,[18,25] or report the presence of cavities[25] and microcracks[19] in the material after deformation. The discrepancies among these observations may be ascribed either to problems having occurred during the preparation of the thin sections or to real differences between the materials. No structural comparison was reported of areas of a single sample being in tension and in compression.

Data obtained from samples deformed in compressive mode are more reliable and easier to interpret, because the geometry and the stress field are better defined. However, such experiments are rarely reported in the literature, probably due to the complexity of the experimental set-up. For example, alumina composites with various whisker contents are studied in compressive creep in Ref. 25: at stresses of 100 MPa, the strain rate varies from $10^{-7}\,s^{-1}$ at 1573 K to $7 \times 10^{-7}\,s^{-1}$ at 1673 K. In Ref. 25 a stress exponent between 1 and 2, and an average activation energy of $620\,kJ\,mol^{-1}$, are reported at temperatures close to 1600 K.

The effect of environment on the creep behaviour of the composite is reported in two investigations. Firstly, creep cracks are observed to form above a threshold value of the tensile strain during bending tests carried out in oxidizing atmosphere.[23] Secondly, no significant difference in strain rate is observed for creep experiments performed in either oxidizing or neutral atmosphere.[25]

In the present paper, the high-temperature compressive creep behaviour of an alumina–zirconia composite reinforced with silicon carbide whiskers is investigated. The influence of temperature, stress, preanneal and environment on the creep properties are studied and related to the transmission electron microscopy observations of the composite microstructure before and after creep, in order to determine the deformation mechanisms and material damage due to creep.

Room-temperature toughness and strength of this three-phase composite are improved, compared to

alumina–silicon carbide composites.[3] The dispersed zirconia particles undergo the well-known transformation toughening mechanism, already reported by Becher for alumina–zirconia[10] and mullite–zirconia–silicon carbide composites.[10] The addition of this transformation toughening and of the whisker toughening confers on the material its unique fracture performances. The objective of this work is to investigate the interaction of the three phases and the role played by the different interfaces during high-temperature creep, to compare the strain rates of the three-phase composite to that of alumina–silicon carbide whisker composites, and to determine the deformation mechanisms.

2 Experimental Procedures

The composite material used for this study was developed by Desmarquest, France, following a process described in detail in Ref. 5. It contains three phases: 62·7 vol.% alumina, 10·9 vol.% zirconia and 26·4 vol.% silicon carbide. It was densified to full density by hot-pressing at much lower temperature than traditional alumina–silicon carbide composites, due to the presence of zirconia, which acts as a sintering aid. Zirconia further acted as a control for the growth of the alumina grains, giving the composite a homogeneous microstructure.

Parallelepipeds of size 3 mm × 3·2 mm × 7 mm were cut out of the material (the hot-pressing axis was parallel to the 3·2 mm side). The two end-faces of the parallelepipeds were polished parallel.

Some samples were used as-received, others were annealed prior to deformation, for 50 to 100 h. The anneal was performed either in neutral atmosphere (embedded in alumina–silicon carbide powder mixtures under argon flow), in oxidizing atmosphere (under air flow) or in reducing atmosphere (embedded in graphite powder).

Compressive creep tests of the different samples described were performed at temperatures between 1500 and 1700 K at stresses between 10 and 200 MPa in oxidizing (air) or neutral (argon) atmosphere. All samples were deformed under constant load in compressive mode. Most samples were successively deformed under different loads or for different temperatures. For microscopy investigations the samples were deformed in only one creep condition.

The constant load creep apparatus used for this investigation was described in detail in Ref. 27. It comprised a furnace with lanthanum chromite heating elements. The load was applied onto the sample via alumina or silicon carbide push-rods. Two silicon carbide platelets (4 mm × 4 mm × 2 mm), much harder than the investigated material, were inserted between the push-rods and the sample ends. The entire set-up was enclosed in a gas-tight alumina tube located inside the furnace, so that the atmosphere around the sample could be controlled. All tests were run under continuous gas flow (argon or air). A thermocouple located near the sample was used to control the furnace temperature. The shortening of the sample was recorded by a direct current deformation transducer. At the end of each experiment, the total recorded deformation was compared to the final length of the sample.

Thin slices were cut parallel and perpendicular to the deformation axis in both undeformed and deformed samples. Some of the slices were polished and observed by scanning electron microscopy (SEM). For transmission electron microscopy observations (TEM), further thinning of the slices by mechanical grinding was necessary, followed by ion-thinning under argon bombardment. The so-prepared thin foils were then coated with a thin carbon film, in order to avoid charging under the electron beam during observation. For TEM observations, special care was taken to keep track of the deformation axis of the sample. A JEOL 2000FX transmission electron microscope equipped with an energy dispersive X-ray detector (EDX) was used for this work.

3 Experimental Results

Before presenting the creep results, a description of the undeformed materials, with or without anneal prior to deformation, will be given.

3.1 Description of the materials

3.1.1 As-received material

In the starting material, the three phases, Al_2O_3, SiC and ZrO_2 (Y_2O_3) (partially stabilized), are homogeneously distributed, the silicon carbide whiskers being preferentially oriented perpendicularly to the hot-pressing axis. Essentially no porosity is visible. X-Ray diffraction confirms (within its detection limit) that no additional phase is present besides alumina, silicon carbide and zirconia. In the typical cross-section shown in Fig. 1, obtained by optical microscopy, the bright phase is zirconia, the light grey phase is silicon carbide and the alumina matrix appears dark grey.

The phase distribution was investigated in greater detail by backscattered imaging in a scanning electron microscope. The zirconia particles appear normally angular, with many irregular corners and an average size of 1 μm. Silicon carbide whiskers have a diameter of about 1 μm and a length varying from 3 to 10 μm. The relatively short whisker size is due to processing, especially to the milling step, which easily fractures the whiskers. The alumina

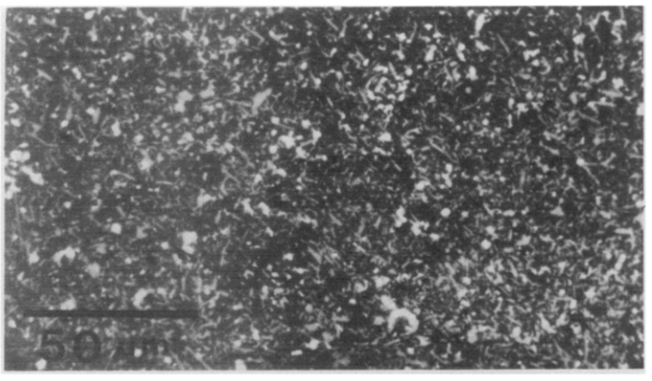

Fig. 1. Optical micrograph of a polished cross-section of Al_2O_3–ZrO_2–SiC composite showing the regular phase distribution (zirconia particles are white, SiC whiskers light grey and alumina dark grey).

grain size is about 1 μm. The typical phase distribution is presented in the scanning electron micrograph of Fig. 2.

TEM observations indicate that silicon carbide whiskers, alumina grains and zirconia grains are in intimate contact (Fig. 3). No interdiffusion zone or formation of new phase can be identified by EDX analysis across the interfaces. Spherical zirconia inclusions are observed in some larger alumina grains. In rare instances, a glassy film can be detected in alumina grain boundaries, but in most cases, even at triple junctions, the alumina grain boundaries and the alumina–zirconia interfaces are free of any glassy layer. The interfaces between silicon carbide whiskers and alumina or zirconia are very sharp: no interdiffusion of silicon into the oxides or of aluminium or zirconium into the silicon carbide can be measured. The corresponding solubilities are probably below the detection limit of the EDX

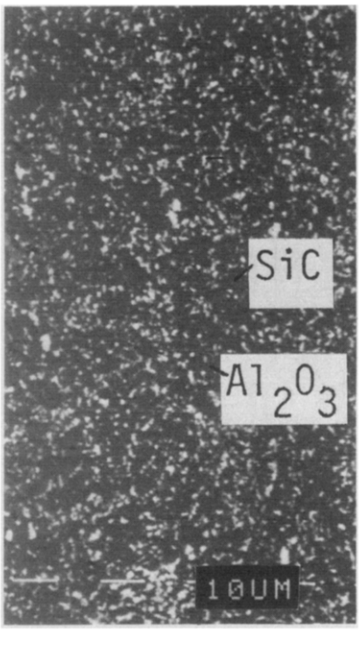

Fig. 2. Scanning electron micrograph of a polished cross-section of the Al_2O_3–ZrO_2–SiC composite showing the morphology of the different phases (zirconia is white, alumina grey and silicon carbide light grey).

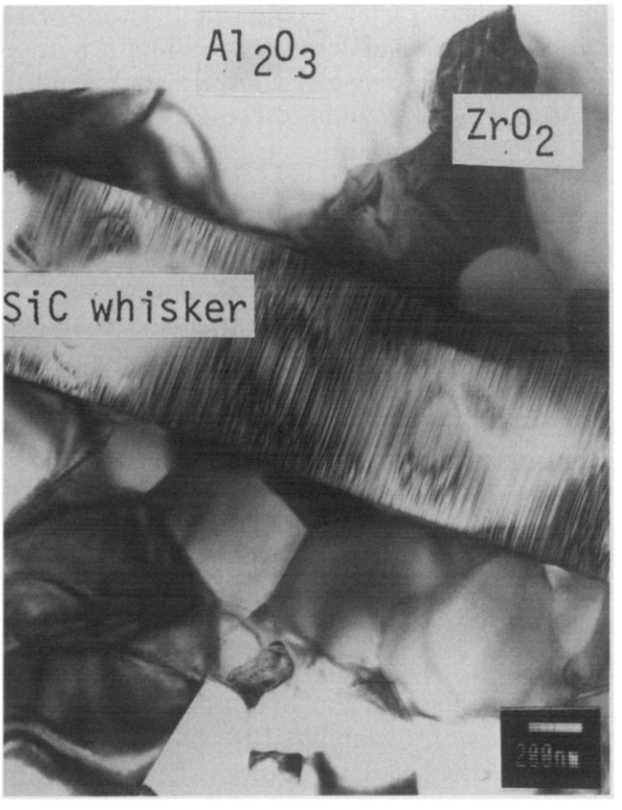

Fig. 3. Transmission electron micrograph of the typical microstructure of the composite: heavily faulted SiC whiskers, light grey alumina matrix grains and dark zirconia grains are in direct contact.

system (0·2%). High-resolution transmission electron microscopy allowed imaging of the very thin amorphous layer at the whisker interfaces: its thickness averages 3 nm.

3.1.2 Material annealed in a neutral atmosphere

The microstructure of the composite annealed in a neutral atmosphere (surrounded by silicon carbide–alumina powder and argon atmosphere) shows no difference to that of the starting material, except for a slight increase of the alumina grain size. In particular, the interface characteristics are unchanged.

3.1.3 Material annealed in an oxidizing atmosphere

Details about kinetics and microstructural changes occurring during the oxidation of the composite are given in Ref. 22. Here, only a brief summary is given. During oxidation, a porous surface scale forms, which is depleted in silicon carbide whiskers and consists of a mixture of mullite, zirconia and alumina. In a very thin intermediate layer below this scale, partially dissolved SiC whiskers, carbon, silica, zircon, zirconia, mullite and alumina coexist. The thickness of the oxidation scale depends on the temperature and duration of the reaction (see Ref. 22).

The parallelepipeds used for the creep tests have been preoxidized for 50 h at 1673 K, conditions for

which the average thickness of the oxidation layer is 60 μm. The bulk of the samples is unaffected by the oxidation process and keeps the characteristics of the starting material, except for a small increase in grain size for alumina.

3.1.4 Material annealed in a reducing environment
During annealing in graphite ampoules, the composite develops a whisker-depleted surface layer. This layer is depleted in silicon, as a result of the evaporation of SiO, and consists of a mixture of aluminium oxycarbides, carbon and alumina. Even for long annealing times and at high temperature the thickness of this scale remains negligible (10 μm after 100 h at 1773 K). Again, the bulk material is not affected by the reduction.

3.2 Creep results

3.2.1 Shape of the creep curve
The shape of the creep curve is identical for the different sample types. Following the initial loading, primary creep takes place to a variable extent, depending on the applied stress and the sample history (nature of the pretreatment). Further loading always yields more limited amounts of primary creep. In all cases, this transient creep part of the curve, characterized by a decreasing strain rate, is followed by a secondary steady-state creep region. For large stresses (>100 MPa), the steady-state part of the creep curve is reached within a few hours, while for low stresses (<40 MPa) it takes up to 50 h for the strain rate to become constant. In the usual test conditions, the ternary stage of the creep curve was never observed, even at strains close to 50% (at 1673 K and 100 MPa)! A typical creep curve is shown in the deformation versus time plot and the corresponding creep rate versus deformation plot of Fig. 4.

A small apparent increase of the steady-state creep rate is sometimes observed after a long time of deformation in an oxidizing (air) atmosphere. This variation is ascribed to microstructural changes in the surface scale which, giving rise to lower hardness than the original material, results in an apparent decrease of the effective sample cross-section, and thus to a higher apparent creep rate. In the same way, a slight increase of the creep rate is measured for samples previously annealed in air (see Section 3.2.2).

3.2.2 Influence of atmosphere and preanneal
In the following, the samples are characterized by the condition of their preanneal and by the nature of the atmosphere used during their deformation by creep:

Type I As-received samples deformed under argon flow.

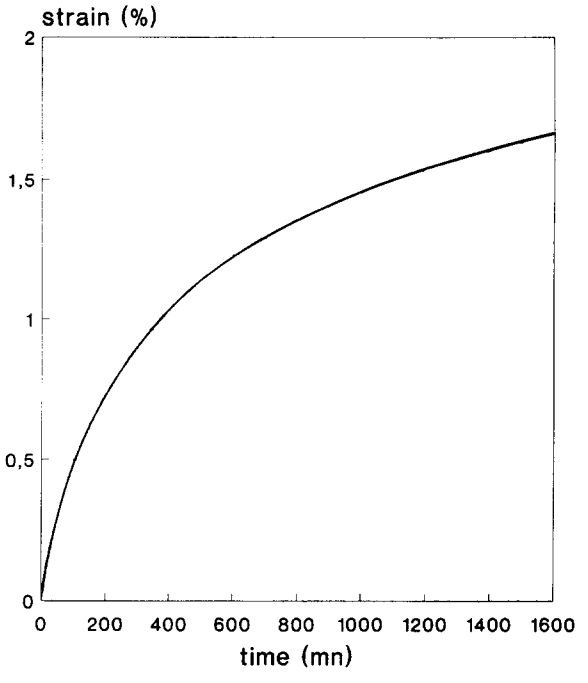

(a)

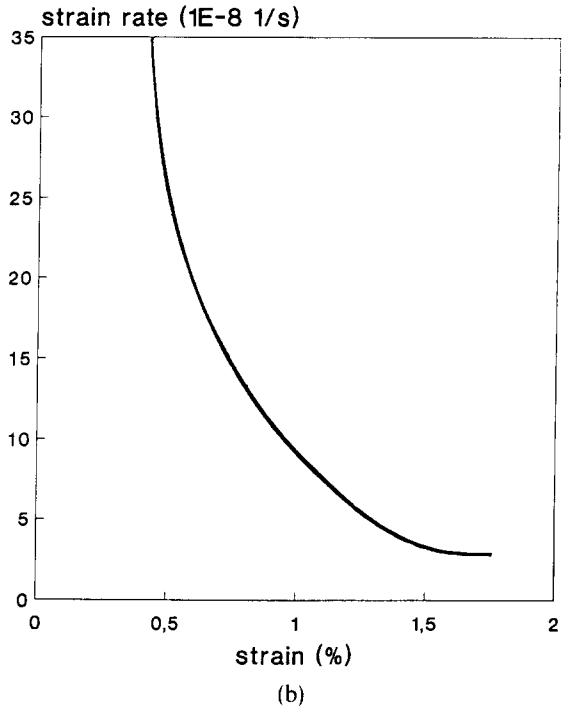

(b)

Fig. 4. Typical creep curve of the composite material at 1600 K, 44 MPa. (a) Strain versus time plot; (b) strain rate versus strain plot.

Type II As-received samples deformed under air flow.

Type III Samples preannealed in argon for 50 h at 1673 K and deformed in an argon flow.

Type IV Samples preoxidized in air for 50 h at 1673 K and deformed in an air flow.

Type V Samples pretreated in a graphite ampoule for 100 h at 1773 K and deformed in an argon flow.

For all sample types the total strain reached during deformation was always less than 3%. Figure 5 is a

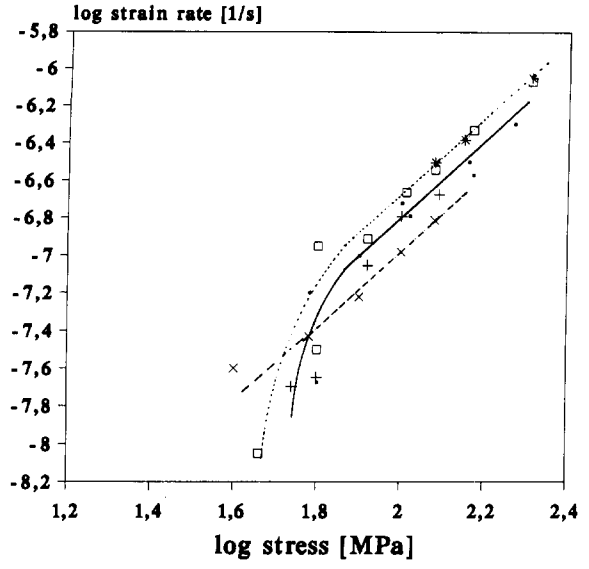

Fig. 5. Strain rate versus stress plot for the composite material deformed at 1573 K in various atmospheres and after different pretreatments. ■, As-received samples deformed under argon flow (type I); ∗, as-received samples deformed under air flow (type II); +, samples preannealed in argon for 50 h at 1673 K and deformed under argon flow (type III); □, samples preoxidized in air for 50 h at 1673 K and deformed under air flow (type IV); ×, samples prereduced in a C/CO buffer for 100 h at 1773 K and deformed under argon flow (type V).

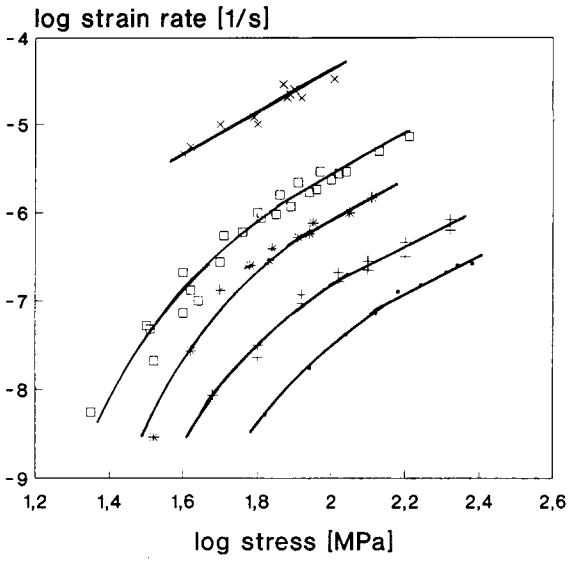

Fig. 6. Strain rate versus stress plot for the composite material at different temperatures. ■, 1550 K; +, 1570 K; ∗, 1600 K, □, 1623 K; ×, 1673 K.

log–log plot of creep rate versus applied stress for the different sample types deformed at 1573 K. The creep curves obtained for samples of types I to V yield similar values of strain rate, which implies that the pretreatment or the atmosphere during creep has, at most, a minor effect on the creep behaviour.

At a given temperature the creep rate was 1·3 times faster when the deformation took place in an oxidizing atmosphere (type II specimens) than when a neutral atmosphere surrounded the samples (type I specimens).

A preoxidation in air induces no further visible shift of the creep rate to higher values, even though the oxidation scale thickness after preoxidation is of the same order of magnitude (60 μm after 50 h at 1673 K) as the scale thickness after a long creep experiment in air (70 μm after 150 h at 1573 K). Apparently the effect of stress during the oxidation anneal is important.

A preanneal in argon (type III specimens) yields only a very small decrease of the strain rate.

A much larger effect is observed when the preanneal was performed in graphite atmosphere (type V specimens): the creep rate is then 1·7 times slower than that of the untreated material.

At this point it is important to emphasize that the differences in strain rate due to the sample treatment are small compared to those related to changes in the temperature or applied stress.

3.2.3 Stress exponent and activation energy

In order to determine the stress exponent in the classical power law approach, $\dot{\varepsilon} = A\sigma^n e^{-Q/RT}$, different loads were consecutively applied at a fixed temperature. In Fig. 6 log–log plots of the strain rate versus stress are presented for temperatures ranging from 1550 to 1673 K. Since the differences in strain rate related to various atmospheres or preanneal conditions are minor compared to temperature or stress effects, only the creep data obtained in air are presented. The creep rate increases drastically with temperature. The stress exponent, which can be computed from the slope of these creep curves, varies with the stress. Above a temperature-dependent threshold stress, $n = 2$ up to 1573 K and 2·5 above 1600 K. Below the threshold stress, the creep rate decreases rapidly with decreasing stress. In this region of the creep curve, the stress exponent may be in excess of 10.

The apparent activation energy, Q, was determined by performing temperature jumps for some samples from 1573 K to 1623 K and then to 1673 K, at constant stress (above the threshold value) and for a constant microstructure: between 1573 and 1673 K the average activation energy is 800 kJ mol^{-1}.

3.2.4 Evolution of the microstructure during creep

Scanning electron microscopy reveals the presence of cavities at about every tenth triple junction of the deformed samples (1573 K, 100 MPa, $\varepsilon = 3\%$) (see Fig. 7). The shape and frequency of these cavities do not depend on the orientation of the sample section, whether they are parallel or perpendicular to the deformation axis. Cavities form at alumina triple junctions and in alumina– or zirconia–whisker interfaces.

After deformation at higher temperature (>1723 K) and at higher stresses the deformed materials contain extended microcracks, in addition to the cavities at triple junctions. These microcracks

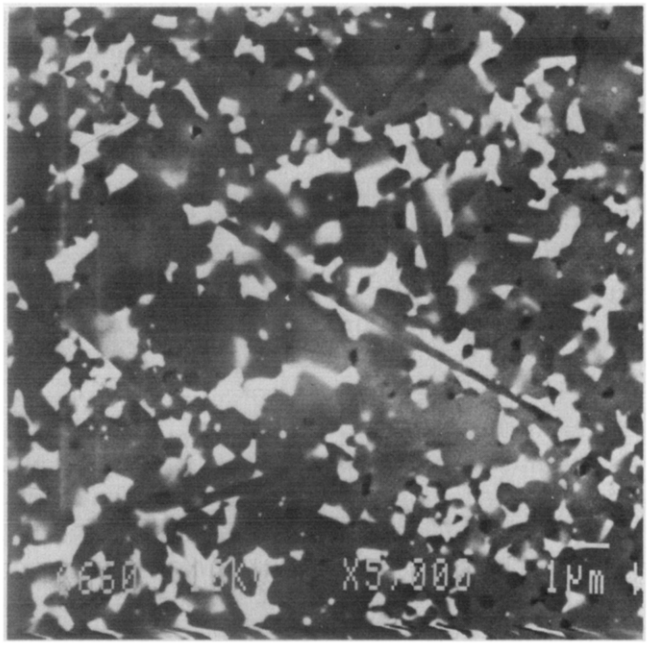

Fig. 7. Scanning electron micrograph of the polished cross-section of a sample deformed at 1573 K, under 100 MPa and up to 3% strain. Cavitation is visible at triple junctions.

propagate along grain boundaries, along silicon carbide whisker interfaces and sometimes cross alumina grains or whiskers.

TEM studies confirm these observations. Regularly shaped cavities with a triangular shape and an approximate diameter of about 20 nm were observed at triple junctions of the matrix, while the cavities detected in the whisker interfaces are often elongated and surround the whisker. The length of this second type of cavities can reach 1 μm, which corresponds to the length of the whisker facets (Fig. 8). Normally, the cavities were not surrounded by any amorphous material.

TEM analysis of samples deformed under 100 MPa at 1673 K confirms the presence of microcracks for these creep conditions. The cracks propagate intra- and intergranularly in the alumina matrix and along the whisker interfaces. The cracks can run for several microns along the whisker interface, before either completely stopping or crossing the whisker at a surface defect (Fig. 9). Detailed analysis of the microcrack location shows that the crack does not propagate in the interface between alumina and silicon carbide but in the alumina phase.

Transmission electron microscopy also reveals a high density of stress whirls at alumina grain boundaries or at whisker interfaces. These whirls are located symmetrically on both sides of a boundary, but shifted with respect to one another.

The general phase distribution inside the sample does not change during creep: the matrix grains keep their average shape; only a small increase in the average grain size of alumina due to the

(a)

(b)

Fig. 8. Transmission electron micrographs of typical areas of samples deformed at 1573 K and under stresses up to 200 MPa, showing (a) cavities at triple junctions; (b) cavitation at whisker interfaces.

Fig. 9. Transmission electron micrograph of a sample deformed at 1673 K under stresses up to 100 MPa, showing microcracks at grain boundaries and along whisker interfaces.

high-temperature annealing is noticed. The silicon carbide whiskers are not bowed; they stay straight even after deformation. Intense microtwinning is observed inside some deformed zirconia grains. Stress concentrations, visible as whirls in TEM, often occur in the surroundings of these grains. It is not clear whether the twinning of zirconia occurs during deformation or during cooling under stress.

The same dislocation density is present in both deformed and undeformed samples. Isolated dislocations created during the material fabrication process could be observed inside some larger alumina grains, especially in the vicinity of the small zirconia inclusions present in these grains. No deformation-induced dislocation network was detected. As a consequence, it can be concluded that dislocations do not play an active part during creep deformation.

4 Discussion

4.1 Transient creep

The presence of a primary creep region, of variable extent, indicates that structural changes occur inside the material during the period following the initial loading. However, the strain during this stage is normally less than 2%, suggesting that the microstructure does not change to a great extent. This indication is confirmed by transmission electron microscopy investigations. Actually, no change in microstructure, like for example the formation of subgrain boundaries or dislocations, was observed. Since the grain size is found to remain fairly constant during this primary creep, this part of the creep curve cannot be explained by grain growth.

The reaction of the material to first loading can then be explained by a reorganization of the composite microstructure under load, during which non-compensated grain boundary sliding occurs upon redistribution of the glassy grain boundary film. The glass layer reorganizes itself in whisker interfaces and in the wetted alumina grain boundaries (more rare) under the effect of the new stress field applied to the sample. A similar primary stage of the creep curve is reported for polycrystalline alumina,[28] but no general explanation is provided.

4.2 Effect of pretreatment and atmosphere

In the heat-treated composite, no significant interdiffusion was observed between the different phases (alumina, zirconia and silicon carbide) up to 1773 K.[22]

Different atmospheres have the following effects:[22] only a small increase in alumina grain size was observed after annealing or creep experiments of long duration in neutral atmosphere, the grain growth of alumina in the composite being inhibited by the presence of zirconia. Consequently, the strain rate was not observed to decrease with annealing or preannealing time in neutral atmosphere.

Annealing the composite in an oxidizing atmosphere yields the growth of a porous oxidation surface scale, as described in Ref. 22. This scale is depleted in silicon carbide whiskers and consists of a mixture of mullite, alumina and zirconia.[22] It is much softer than the starting composite (softening estimated to a factor 100). After the preanneal in air, the thickness of this layer is about 60 μm, corresponding to an effective cross-section decrease from 9·6 to 9·17 mm^2. After a 150 h creep experiment at 1573 K, the layer thickness is 70 μm for a sample without preannealing treatment and 100 μm in the case of preannealed (in air) samples (effective cross-section of 9·0 mm^2).

Having calculated these effective reductions of cross-section, it is possible to correct accordingly the measured values of the strain rate. The increase in strain rate by a factor 1·3 measured for creep in air compared to creep in a neutral atmosphere can, however, not be entirely explained by this correction. It is proposed that the oxidation kinetics may be faster under stress, the oxidation taking place by

rapid transport through the glassy grain boundary and whisker interfacial film. Oxygen penetrates rapidly along this film and oxidizes the adjacent grains. Under the influence of the external stress, the glassy phase is redistributed and, therefore, wets even more boundaries. In summary, the amount of glassy film increases continuously during oxidation and leads, firstly, to a longer transient creep (with redistribution of this glassy phase) and, secondly, to an additional strain rate increase during secondary creep.

A preanneal in reducing atmosphere, performed at 1773 K for 100 h in a graphite crucible, yields as well a surface layer depleted in SiC whiskers, which consists of alumina and mixed silicon–aluminium oxycarbides. These compounds are again much softer than the starting material, but the thickness of the reduction layer after the anneal is only 10 μm. However, this surface layer cannot account for the fact that a lower strain rate was observed for this type of pretreated samples relative to those treated (anneal + creep) in a neutral atmosphere. A thinning of the interfacial film could be proposed to explain this behaviour. The following model would account for such a thinning. It is well known that carbon can easily diffuse along interfaces or grain boundaries in oxides[30] and in wetted grain boundaries in non-oxides.[31] It can penetrate in the wetted boundaries of the composite and react with the glassy film to reach equilibrium:

$$Al_xSi_{1-x}O_y + C \rightarrow Al_2O_3 + SiC + CO$$

The carbon monoxide formed according to this reaction would diffuse along the interfaces. As a result of the reaction, the thickness of the intergranular film decreases to a minimum equilibrium value, not only inside the reduction scale but also inside a much thicker layer, which is affected by the diffusion of carbon. Such a decrease of the thickness of this glassy whisker interfacial film would account for the reduced secondary creep rate, making grain boundary sliding more difficult, especially in the neighbourhood of the whiskers, where the interfacial layer would be missing or much thinner.

To summarize the above discussion, it should be remembered that preannealing and the nature of the atmosphere have a limited impact on the creep behaviour of the composite studied in this work, but may play a more important role in the case of materials containing a larger amount and/or thicker glassy grain boundary films. This is clearly shown by the study in Ref. 26, where the effect of oxidizing atmosphere on the strain rate is more important than in the present case. No results on the stabilizing effect of a reducing atmosphere are available in the literature for comparison with the present measurements. However, a similar effect was reported in Ref. 14, where composites fabricated with differently pretreated whiskers are compared: composites made of whiskers previously reduced, in order to eliminate the amorphous surface layer, gave better creep results than materials with preoxidized whiskers (due to the presence of a thick amorphous interfacial film).

4.3 Stress exponent and activation energy

The composite material has a complex creep behaviour. The stress exponent, n, varies with temperature and stress, indicating the contribution of several deformation mechanisms.

Especially at low stresses, a steep part can be observed at all temperatures in the $\log \dot{\varepsilon}$–$\log \sigma$ curve. Such behaviour was ascribed to grain growth occurring during long lasting creep experiments performed with polycrystalline Al_2O_3.[32] However, this explanation does not apply to the present case, since no grain size increase could be identified by TEM in the deformed material and no strain rate variation could be measured upon load cycling of a given sample. It is proposed that this increase in the slope of the creep curve at low stress may be related to the existence of an interfacial reaction, which would become slower with decreasing stress. Similar observations are reported in Ref. 33 and interpreted, as for metals, as a stress threshold value for creep to occur. It is thought that, in the present case, it can rather be interpreted as an energy barrier for the creation or annihilation of vacancies at interfaces.

In an intermediate stress range, a stress exponent of 2 was measured, up to 1600 K. Above this temperature it increases to 2·5. SEM and TEM observations of samples deformed under these conditions indicate, firstly, that cavitation occurs occasionally at triple junctions and, secondly, that stress whirls are present at interfaces and grain boundaries. Furthermore, no additional dislocations could be detected after deformation. It follows that dislocation creep can be ruled out as a possible controlling mechanism for creep. The presence of cavities in the deformed material is the evidence that cavitation mechanisms contribute to the deformation; however, cavitation does not appear to be the major mechanism, since the density of cavities observed by SEM cannot account for the several percentage strains sometimes recorded.

The stress whirls observed in two adjacent grains are often shifted with respect to each other, indicating that grain boundary sliding is a likely contributing mechanism. The presence of these whirls is a further indication that grain boundary sliding does not occur as easily as in materials containing a large amount of glassy phase. Boundary steps or impurities may be local reasons for these stress agglomerations.

It is concluded that the material deforms by a diffusion-compensated mechanism, where grain boundary sliding is accommodated by grain boundary and interface diffusion. Even though an amorphous phase was only rarely detected in alumina grain boundaries, alumina–zirconia interfaces or triple junctions, these locations, together with the amorphous film located along the whisker interfaces, constitute weak zones of the composite material, where local stress concentrations can occur during creep and lead to the formation of cavities. This conclusion is supported by the direct observation of cavities at some triple junctions and whisker interfaces in the deformed material.

The stress exponent of 2, measured at low stresses and low temperatures, does not correspond to a purely diffusional mechanism, usually associated to a stress exponent of one in monolithic ceramics. It can be ascribed either to the limiting role played by the interfacial reaction of creation or annihilation of vacancies or by the contribution of the cavitational mechanism, which compensates grain boundary sliding.

At the higher temperatures and in the higher stress range, the stress exponent is larger than 2. Samples deformed under such conditions contain a higher concentration of cavities, as well as inter- and intragranular microcracks. The higher stress exponent can therefore be related to more extensive cavitation and to the occurrence of microcracking at these higher stresses.

The special mechanisms proposed by Porter in Ref. 18 for composites containing a high whisker content, whereby bowing of whiskers would occur in a system of connected whiskers, could not be confirmed by the present TEM observations.

The activation energy calculated from the creep studies, of the order of 800 kJ mol^{-1} at 1573 K, is different from that for pure alumina (400–500 kJ mol^{-1})[34] and pure zirconia (600 kJ mol^{-1}).[34] The value is also higher than that reported by Lipetzky *et al.*[26] for an alumina composite containing 33% silicon carbide whiskers. These latter authors reported for the same temperature range as studied in the present work: (i) a low stress regime with a stress exponent $n=1$ and an activation energy of 450 kJ mol^{-1}, and (ii) a high stress regime with a stress exponent $n=5$ and an activation energy of 500 kJ mol^{-1}. A comparison of the present creep data with these literature results obtained by four-point bending tests is hardly possible, since it is well known that for fine-grained ceramics different creep mechanism or different repartition of the mechanisms can take place in tensile and in compressive mode. For the same reason, it is difficult to compare the creep data to those reported in Ref. 35 and obtained by four-point bending of alumina composites with 18 or 30 vol.% silicon carbide; in this case, the reported creep rates are higher, but the stress exponents are similar to those of the present study. Since creep rates derived from flexure tests (compressive and tension mode) are normally higher than those obtained in pure compression mode, it is possible to conclude that the creep rate of alumina–zirconia–silicon carbide composites is somewhat higher than that of pure alumina–silicon carbide composites. An explanation may be found in the fact that, for given creep conditions, pure alumina deforms at a slower rate than pure zirconia.[33] Since the matrix of the material studied here consists partially of zirconia, the increase of creep rate compared to that reported in Refs 4, 19 and 34 may well be related to the creep properties of zirconia.

In any case, the creep rate of the alumina–zirconia–silicon carbide whisker composite is far slower than that of pure alumina with comparable grain size and additives.[29,33] Cannon *et al.*[33] report flexural creep rates of the order of 2×10^{-5} s^{-1} for 100 MPa and 1591 K and 2×10^{-4} s^{-1} for 100 MPa and 1691 K. These authors interpret the observed variation of stress exponent from $n=2$ at low stresses (100 MPa) to $n=1$ at higher stresses by diffusional creep, with grain boundaries acting as perfect sinks/sources of vacancies (corresponding to $n=1$), or diffusional creep with some interface controlled processes or non-accommodated grain boundary sliding (yielding $n=2$).

For the present experimental conditions, the deformation map of Ref. 31 predicts diffusional creep for pure polycrystalline alumina, with a stress exponent of about $n=1$. Compared to pure alumina the present composite material deforms by additional mechanisms like cavitation or microcracking, due to the presence of a weak glassy film at the whisker interfaces and to the different (probably less uniform) stress distribution in the composite interfaces.

5 Conclusions

The behaviour of an alumina–zirconia–silicon carbide whisker composite at high temperature, under stress and in various atmospheres, was studied. Different preanneals showed that the three phases within the composite can coexist and that no interfacial reactions occur in the investigated temperature range. Only a small increase of the alumina grain size was measured. In oxidizing or reducing atmosphere, the composite degrades by slow build-up of a thin outer reaction scale, which is in both cases depleted in silicon carbide whiskers and mechanically less strong than the original material. The creep rate of oxidized samples was

found to be slightly higher than that of the original material, while the opposite relationship was measured for the reduced samples. The small effect resulting from either a preanneal of the sample or the nature of the atmosphere during creep is related to changes of the quality and quantity of the amorphous phase in whisker interfaces and grain boundaries.

Microstructural analysis of the deformed composite materials revealed the presence of cavities at triple junctions or at whisker interfaces, of inter- and intragranular microcracks, and of stress whirls at some grain boundaries. No dislocation activity related to creep could be identified. Since the quantity of cavities is not large enough to account for the observed strain, it is concluded that grain boundary sliding is the major contributing mechanism and is mostly compensated by diffusion and only partially by cavitation.

The high-temperature compressive creep rate of the studied alumina–zirconia–silicon carbide whisker composite is far below the creep rate of pure alumina with similar grain size, but only slightly higher than that of alumina–silicon carbide whisker composites with similar whisker content.

Acknowledgements

The authors are grateful to Desmarquest for supplying the composite material and to M. Cales (Desmarquest) for his collaboration during this project. They further want to thank J. Deschamps and B. Pellissier for their technical support of this work, and gratefully mention the financial support from the French Ministère de la Recherche et de la Technologie.

References

1. Evans, A. J., Perspective on development of high toughness ceramics. *J. Am. Ceram. Soc.*, **73** (1990) 187.
2. Becher, P. F. & Wei, G. W., Toughening behavior in SiC-whisker-reinforced alumina. *J. Am. Ceram. Soc.*, **67** (1984) C267.
3. Homeney, J., Vaughn, W. L. & Ferber, M. K., Pressing and mechanical properties of SiC-whisker–Al_2O_3 matrix composites. *Am. Ceram. Soc. Bull.*, **67** (1987) 333.
4. Porter, J. R. & Chokshi, A. H., Creep performance of silicon carbide whisker reinforced alumina. In *Proceedings of the Int. Conf. Ceramic Microstructure '86: Role of Interfaces*, ed. J. A. Pask & A. G. Evans. *Mat. Sci. Research*, Vol. 21, 1986, p. 237.
5. Cales, B., Mathieu, P. & Torre, J. P., Preparation and characterization of whisker reinforced toughened alumina. In *Proceedings of the 14th Int. Conf. Science and Ceramics*, Canterbury, 1987.
6. Backhaus-Ricoult, M., Castaing, J. & Routbort, J., Creep of SiC whisker reinforced Si_3N_4. *Rev. Phys. Appl.*, **23** (1988) 239.
7. Buljan, S. T., Baldoni, J. G. & Huckabee, M. L., Si_3N_4–SiC composites. *Am. Ceram. Soc. Bull.*, **66** (1987) 347.
8. Lundberg, R., Kahlman, L., Pompe, R. & Carlsson, R., SiC reinforced Si_3N_4 composites. *Am. Ceram. Soc. Bull.*, **66** (1987) 330.
9. Ruh, R., Mazdiyasni, K. S. & Mendiratta, M. J., Mechanical and microstructural characterization of mullite and mullite–SiC whisker and ZrO_2-toughened mullite–SiC composites. *J. Am. Ceram. Soc.*, **71** (1988) 503.
10. Becher, P. F. & Tiegs, T. N., Toughening behavior involving multiple mechanisms: whisker reinforcement and zirconia toughening. *J. Am. Ceram. Soc.*, **70** (1987) 651.
11. Billmann, E. R., Mehrotra, P. K., Schuster, A. F. & Beegly, C. W., Machining with Al_2O_3–SiC-whisker cutting tools. *Ceram. Bull.*, **67** (1988) 1016.
12. Homeny, J. & Vaughn, W. L., Whisker reinforced ceramic matrix composites. *MRS Bulletin*, **15** (1987) 66.
13. Shaw, M. C. & Faber, K. T., Temperature toughening in whisker reinforced ceramics. In *Proceedings of the Int. Conf. Ceramic Microstructure '86: Role of Interfaces*, ed. J. A. Pask & A. G. Evans. *Mat. Sci. Research*, Vol. 21, 1986, p. 929.
14. Becher, P. F., Hsueh, C. H., Angelini, P. & Tiegs, T. N., Toughening behavior in whisker-reinforced ceramic matrix composites. *J. Am. Ceram. Soc.*, **71** (1988) 1050.
15. Tiegs, T. N. & Becher, P. F., Sintered Al_2O_3–SiC-whisker composites. *Am. Ceram. Soc. Bull.*, **67** (1987) 339.
16. Ruehle, M., Dagleish, B. J. & Evans, A. G., On the toughening of ceramics by whiskers. *Scripta Met.*, **21** (1987) 681C.
17. Kriven, W. M., Tendeloo, G. V., Tiegs, T. N. & Becher, P. F., Effect of high temperature oxidation on the microstructure and mechanical properties of whisker reinforced ceramics. In *Proceedings of the Int. Conf. Ceramic Microstructure '86: Role of Interfaces*, ed. J. A. Pask & A. G. Evans. *Mat. Sci. Research*, Vol. 21, 1986, p. 939.
18. Porter, J. R., Observation of non-steady-state creep in SiC whisker reinforced alumina. In *Proceedings of the Conference Whisker and Fiber Toughened Ceramics*, Oak Ridge, 1988.
19. Chokshi, A. H. & Porter, J. R., Creep deformation of an alumina matrix composite reinforced with silicon carbide whiskers. *J. Am. Ceram. Soc.*, **68** (1985) C144.
20. Porter, J. R., Lange, F. F. & Chokshi, A. H., Processing and creep performance of SiC reinforced alumina. *Am. Ceram. Soc. Bull.*, **66** (1987) 343.
21. Solomah, A. G., Reichert, W., Rondinella, V., Esposito, L. & Toscano, E., *J. Am. Ceram. Soc.* (in press).
22. Backhaus-Ricoult, M., Oxidation behavior of a silicon carbide whisker reinforced alumina–zirconia composite. *J. Am. Ceram. Soc.*, **74** (1991) 1793.
23. Jakus, K. & Nair, S. V., Nucleation and growth of crack in SiC–Al_2O_3 composites. *Composites Sci. and Techn.*, **37** (1990) 279–97.
24. Lin, H. T. & Becher, P. F., Creep behavior of a SiC-whisker reinforced alumina. *J. Am. Ceram. Soc.*, **73** (1990) 1378.
25. Arellano-Lopez, A. R., Cumbrera, F. L., Dominguez-Rodriguez, A. & Goretta, K. C., Compressive creep of SiC reinforced Al_2O_3. *J. Am. Ceram. Soc.*, **73** (1990) 1297.
26. Lipetzky, P., Nutt, S. R., Koetser, D. A. & Davis, R. F., Atmospheric effects on compressive creep of SiC-reinforced alumina. *J. Am. Ceram. Soc.*, **74** (1991) 1240.
27. Becher, P. F., Slow crack growth behavior in transformation toughened Al_2O_3–ZrO_2 (Y_2O_3) ceramics. *J. Am. Ceram. Soc.*, **66** (1983) 485.
28. Gervais, H., Pellissier, B. & Castaing, J., Creep apparatus for high temperature and defined atmosphere. *Rev. Int. Hautes Temp. Refract.*, **15** (1987) 43.
29. Chokshi, A. H. & Porter, J. R., High temperature mechanical properties of single phase alumina. *J. Mat. Sci.*, **21** (1986) 705.
30. Grabke, H. J., Solid–gas and solid–solid interfaces of ceramic oxides at high temperatures. In *Conference Proceedings Surfaces and Interfaces of Ceramic Materials*,

ed. L. C. Dufour, C. Monty & G. Petot. NATO ASI Series Vol. 173, 1989, p. 599.
31. Ramoul-Badache, K., Influence de SiC sur la microstructure et la resistance au fluage de Si_3N_4 fritté avec Al_2O_3 et Y_2O_3. Thesis, Lab. Physique des Matériaux, Meudon, France, 1989.
32. Duclos, R. & Crampon, J., Diffusional creep of a SiC whisker reinforced alumina/zirconia composite. *Scripta Met.*, **23** (1989) 1673.
33. Cannon, W. R. & Langdon, T. G., Creep of ceramics. Part I: Mechanical characteristics. *J. Mat. Sci.*, **18** (1983) 1.
34. Lipetzky, P., Nutt, S. R. & Becker, P. F., Creep behavior of an Al_2O_3–SiC composite. In *Conference Proceedings MRS Meeting*, 1988, p. 271.
35. Xia, K. & Langdon, T. G., The mechanical properties at high temperatures of SiC reinforced alumina. In *Conference Proceedings MRS Meeting*, 1988, p. 273.